Contents lists available at ScienceDirect

Thin Solid Films

Nanocolumnar ZrCu thin film metallic glass with tailored mechanical and electrical properties

Evgeniy Boltynjuk [a],[*] , Francesco Bignoli [b] , Sree Harsha Nandam [c] , Damien Faurie [b] , Alexander Welle [d] , Robert Kruk [a] , Philippe Djemia [b] , Horst Hahn [a],[e] , Yulia Ivanisenko [a] , Matteo Ghidelli [b]

[a] Institute of Nanotechnology, Karlsruhe Institute of Technology, Eggenstein-Leopoldshafen, Germany
[b] Laboratoire des Sciences des Procédés et des Matériaux (LSPM), CNRS, Université Sorbonne Paris Nord, Villetaneuse, France
[c] Department of Metallurgical Engineering, Indian Institute of Technology (BHU), Varanasi, India
[d] Karlsruhe Nano Micro Facility and Institute of Functional Interfaces, Karlsruhe Institute of Technology, Eggenstein-Leopoldshafen, Germany
[e] Department of Materials Science and Engineering, University of Arizona, Tucson, United States

ARTICLE INFO

ABSTRACT

Thin-film metallic glasses (TFMGs) are promising materials for flexible electronics due to their large deformability and metallic-like electrical conductivity. Here, we synthesize homogeneous and nanocolumnar ZrCu TFMGs with tailored column size ranging from 16 up to 60 nm, investigating the relationship among atomic structure, electrical and mechanical properties focusing on their potential applications in flexible electronics. Tracer diffusion experiments indicate an absence of macroscopic cracks and enhanced diffusion coefficient for nanocolumnar TFMGs, up to one order of magnitude higher than in homogeneous counterpart, due to the presence of intercolumnar interfaces. We show that electrical resistivity increases with decreasing column size (from 570.0 ± 11.6 down to 285.9 ± 12.6 μΩ × cm) due to the enhanced electron scattering events at intercolumnar interfaces. Tensile tests on polymeric substrates reveal that the crack onset strain increases from 0.8 ± 0.05 up to 1.6 ± 0.05 % for large diameter nanocolumns due to the lower density of intercolumnar interfaces and presence of strong Cu-Cu bonds. Overall, we show how nanoengineering design concepts can be applied to TFMGs to tune their mechanical and electrical performance by controlling the nanocolumnar growth, paving the way for their potential applications in flexible electronics.

1. Introduction

In the last decades, flexible electronics has shown an impressive growth with a potential beyond what is possible with conventional semiconductor based electronics [1–3]. The materials requirements for flexible electronics include the large stretchability without incurring damage as well as high electrical conductivity (retained after deformation) as well as thermal stability and wear/fatigue resistance [1,3].

Thin film metallic glasses (TFMGs) are emerging as a promising material for use in flexible electronics, offering promising combination of mechanical and electrical properties. Unlike crystalline metals, TFMGs lack a long-range ordered structure, which imparts them with superior strength and significantly higher elastic limits compared to crystalline metals and alloys [4,5]. For instance, freestanding ZrNi TFMGs show homogeneous deformation with a combination of

outstanding yield strength up to ~3.5 GPa and fracture strain greater than 14 % (5 % elasticity and >9 % plasticity) [6]. Moreover, metallic glasses (MGs) possess metallic-like electrical resistivity >100 μΩ × cm slightly dependent on the composition [7,8] which is usually ~two orders of magnitude larger than that of crystalline counterparts [8]. However, this drawback is compensated by MG's very low (and sometimes negative) temperature coefficient of resistivity (TCR) meaning that, contrary to crystalline materials, their electrical resistivity decreases when increasing temperature, while ensuring a very stable electrical behavior [9].

The promising combination of mechanical/electrical properties makes TFMGs suitable candidates for flexible electronics. Xian et al. [10] fabricated a strain sensor depositing ZrCuNiAl on a flexible substrate, reporting large piezoresistance with a gauge factor of ~2.86, an elastic limit (>1 %) higher than that of crystalline alloys and excellent

conductivity ($>5 \times 10^3 \ S \times cm^{-1}$), extremely low TCR value ($9.04 \times 10^{-6} \ K^{-1}$) and antibacterial properties, suitable for medical applications. Similarly, Glushko et al. [11] performed tensile test of PdSi TFMG on polymeric substrate, reporting pronounced size effect resulting in extended crack-free deformation up to 6 % strain for ultra-thin (7 nm) thickness, with an exceptional cyclic reliability sustaining cyclic strains of 3 % up to at least 30,000 cycles without any fatigue damage or electrical conductivity degradation. Jung et al. [12] produced amorphous FeZr-integrated sensor on a flexible platform demonstrating high range of pressure sensitivity (100 – 5000 Pa), temperature sensitivity (~150 °C), photo responsivity (400 – 550 nm) levels, capable of functioning as a high-performance heater (~ 80 °C). Finally, nanostructured ZrCu TFMGs (constituted by nanoclusters) have been produced by pulsed laser deposition (PLD), reporting outstanding and tunable mechanical/electrical properties [13], including a yield strength (up to ~2 GPa) and large total elongation to failure (>9 %) [13] and sheet resistance of 3.0 Ω/sq with application for flexible thermotherapy patches [14].

However, few studies dealing with the synthesis of advanced TFMG architectures, involving a fine control of the sub-microscale morphology aimed to tune and boost both mechanical and electrical properties as well as the adhesion on a polymeric substrate with a specific focus to achieve property combinations relevant for flexible electronic applications. Here, we synthesized nanocolumnar ZrCu TFMGs with tailored column sizes (from 16 up to 60 nm) and investigate the correlation between their structure and mechanical/electrical behavior, especially involving tensile tests on polymeric substrate with specific implementation for flexible electronics applications.

2. Materials and methods

2.1. Thin films synthesis

Compact and nanocolumnar ZrCu TFMGs were deposited using radio frequency (RF) and direct current (DC) magnetron sputtering chambers.

Thin film samples deposited by RF sputtering were prepared from an alloy target of nominal composition of $Zr_{40}Cu_{60}$ (at. %). The disk-shaped target, with diameter of 50.8 mm and thickness of 5 mm, was mounted 100 mm from the substrate at a fixed tilt angle of 20°. The background pressure before deposition was below 5.0×10^{-6} Pa. Sputtering was performed with the temperature of substrate of 293 K and power of 100 W with substrate rotation velocity of 10 rpm. Films of two types: homogeneous and columnar with columns of 16 nm were prepared. Homogeneous films were deposited at working pressure of 2.8×10^{-1} Pa and constant Ar flow rate of 40 sccm. Columnar films with 16 nm columns were deposited at working pressure of 8×10^{-1} Pa and constant Ar flow rate of 100 sccm.

Thin film samples deposited by DC sputtering were prepared using two pure targets of Cu and Zr, each with a diameter of 76.2 mm and thickness of 5 mm, in mirror-field configuration varying applied power. The sputtering system was used with a fixed distance between the substrate and target of 100 mm and target tilt angle of 38°. The background pressure before deposition below 5.0×10^{-6} Pa was reached in the chamber. Thin films were deposited continuously on both Si (100) wafers with a native oxide layer and Kapton®. Sputtering was performed with the temperature of substrate of 293 K without the rotation of the substrate with a constant Ar flow rate of 100 sccm. Power applied to targets were varied to obtain films with various sizes of columns. Films with 40 nm columns were obtained using: 45 W for Cu target, 100 W for Zr target and working pressure of 8×10^{-1} Pa. Films with 60 nm columns were obtained using: 80 W for Cu target, 100 W for Zr target and working pressure of 8×10^{-1} Pa.

Films were deposited on Kapton® and Si (100) + 300 nm thick SiO_2 substrates. Samples deposited on Kapton® strips were used for tensile tests, while structural and electrical measurements were performed on films deposited on Si (100) + 300 nm thick SiO_2 substrates. Sputtering

times were chosen to obtain films with a thickness of 400 nm. Thickness of samples was measured by Veeco Dektak 6 M Stylus Profiler and by scanning electron microscopy (SEM LEO 1530, Carl Zeiss AG). Table 1 summarizes the most important synthesis parameters as well as the chemical composition of prepared TFMGs.

2.2. Structural characterisation

Scanning electron microscope LEO 1530, Carl Zeiss AG equipped with an energy dispersive X-ray (EDX) detector (Oxford Instruments) was used to inspect morphology and determine atomic composition of thin films (using AZTEC software, Oxford, Instruments). EDX measurements were performed on several areas using accelerating voltage of 20 kV and working distance of 8.5 mm. X-ray diffraction (XRD) measurements were carried with D8 Discover powder diffractometer in grazing incidence mode using Cu-Kα radiation (λ=0.154 nm). Measurements were performed in 25–65° 2θ range with grazing angle of 0.5° using continuous scan mode with step size of 0.03° and time per step of 4 s.

2.3. Tracer diffusion measurements using time-of-flight secondary ion mass spectrometry (ToF-SIMS)

ToF-SIMS measurements were performed on homogeneous and columnar samples with columns of 16 nm using a Fe-tracer layer applying a TOF5 Secondary Ion Mass Spectrometer manufactured by Iontof, Münster, Germany. A thin Fe layer was deposited near the mid-plane of 400 nm thick samples by cosputtering from a magnetron gun equipped with a pure Fe target. Sputtering of ZrCu films was not interrupted during the process of film preparation, while the shutter for the gun containing Fe target was shortly opened to sputter a 1 nm thick Fe layer. Such procedure allows distribution of tracer atoms in a ~3 nm thick layer of ZrCu, preventing formation of discrete interfaces and possible contaminations [15].

The diffusion annealing was performed using a vacuum furnace at 573 K for a duration of 3.45×10^5 s. The temperature was controlled using a Chromel-alumel thermocouple with an accuracy of ± 2 K. The base pressure prior to annealing was below 1×10^{-6} Pa, and during the annealing, the pressure remained around 5×10^{-6} Pa. SED EDX performed on annealed samples showed that the Zr to Cu atomic ratio remained unchanged within experimental error, and no O_2 peak was detected. XRD patterns of the annealed samples showed no crystalline peaks, supporting that the films remained fully amorphous.

Concentration-depths profiles of Fe were determined using dual beam depth profiling. A 25 keV Bi^+ primary ion beam was scanned over a field of view of 100 × 100 μm^2 for spectrometry ("high current bunched mode"), while the sample was continuously eroded by a sputter beam of 1 keV O_2^+ scanned over a concentric area of 250 × 250 μm^2. The high mass resolution, 8000 m/Δm, allowed for a separation of adjacent signals like $^{56}Fe^+$ (55.9344 m/z) and $^{28}Si_2^+$ (55.9533 m/z). Secondary ions (64 × 64 pixel) were collected and from the obtained raw data sets a region of 50 × 50 μm^2 was selected showing well defined interfaces. Depth calibration was obtained from the total film thicknesses, see Sample Preparation. Heat treated samples showed a broadening of the iron profiles (sum of ^{54}Fe and ^{56}Fe) due to diffusion, depending on time and temperature of the heat treatments of the samples, but depth integrated (total) iron signals stayed constant within each sample set, indicating that the SIMS matrix effect is not significantly affecting the Fe quantification in this case.

2.4. Tensile tests on flexible substrates

Tensile tests were performed on films deposited on flexible Kapton® substrates, using a 300 N Deben tensile machine combined with a Keyence confocal microscope for in-situ observation. The films were deposited on one side of Kapton rectangular coupons with a length of 40 mm, width of 1.5 mm and thickness of 0.18 mm. The specimens were

Table 1

Synthesis parameters of homogeneous and nanocolumnar ZrCu TFMGs and their chemical compositions measured by SEM/EDX.

Sample	Sputtering conditions	Working pressure, Pa	Working power, W	Deposition rate, nm/min	Chemical composition, at. %	
					Cu	Zr
Homogeneous	RF, binary target	2.8×10^{-1}	100 for ZrCu	8.3	58.55 ± 0.38	41.45 ± 0.38
16 nm columns	RF, binary target	8×10^{-1}	100 for ZrCu	6.3	56.38 ± 0.48	43.62 ± 0.48
40 nm columns	DC, two targets	8×10^{-1}	45 for Cu, 100 for Zr	13.3	54.69 ± 0.31	45.31 ± 0.31
60 nm columns	DC, two targets	8×10^{-1}	80 for Cu, 100 for Zr	20.3	68.69 ± 0.28	31.31 ± 0.28

gripped at both ends and pulled uniaxially along their length. The tensile speed (v_t) was 8.3×10^{-3} mm/s and sample gauge length was 25.4 mm, corresponding to a strain rate of ca. 3.3×10^{-4} s^{-1}.

To monitor crack formation, the tests were periodically paused at predefined strain increments, allowing for the acquisition of images using 10×, 20×, and 50× objectives. This enabled visualization of a sufficient number of cracks in order to determine their linear density. To quantify crack density, the number of cracks was counted in the microscope field of view. And the linear density of cracks (in the direction orthogonal to the applied load) was calculated as the number of cracks over the area of the sample captured by the microscope objective. This procedure was repeated at each strain increment to capture the evolution of crack density. Strain was determined as:

$$\varepsilon = \frac{\Delta l}{l} * 100\% \qquad (1)$$

where Δl is the actuator displacement (measured with an accuracy of 0.001 mm) and l is the sample gauge length.

The crack onset strain (COS) value was defined as the strain at which the first through-width cracks appeared in the field of view. COS was determined by examining the image sequence acquired during the test and identifying the earliest strain at which visible cracking occurred. Two samples for each state were measured to determine COS and the evolution of the linear density of cracks, and an average value of strain was calculated.

2.5. Electrical resistivity measurements

The electrical resistivity has been measured by Van der Pauw method using a Keithley 4200A-SCS parameter analyzer. Square area of 4 × 4 mm^2 was cut on each film with a TRUMPF TruMicro 5000 laser system.

3. Results

3.1. Microstructure

Fig. 1 are representative SEM micrographs capturing the structural characteristics of homogeneous and nanocolumnar ZrCu TFMGs, highlighting the significant variations observed in column diameters, which range between 16 and 60 nm. Low deposition pressure (2.8×10^{-1} Pa) promotes the formation of a homogeneous film (Fig. 1a, e), distinguished by its smooth, continuous morphology without of any notable columnar features. In contrast, the progressive increment of the deposition pressure up to 8×10^{-1} Pa results in a dramatic shift in morphology, producing a distinct columnar structure (Fig. 1b, f) with an average column's diameter of ~16 nm (Fig. 1i).

Further refinements of synthesis parameters, including controlled variations in working pressure, working power, and substrate temperature, were explored to evaluate their influence on column morphology and average diameter. However, these variations had a minimal effect for thin films fabricated under the RF sputtering configuration, as shown in Table A1, Fig. A1. In contrast, significant improvements in the ability
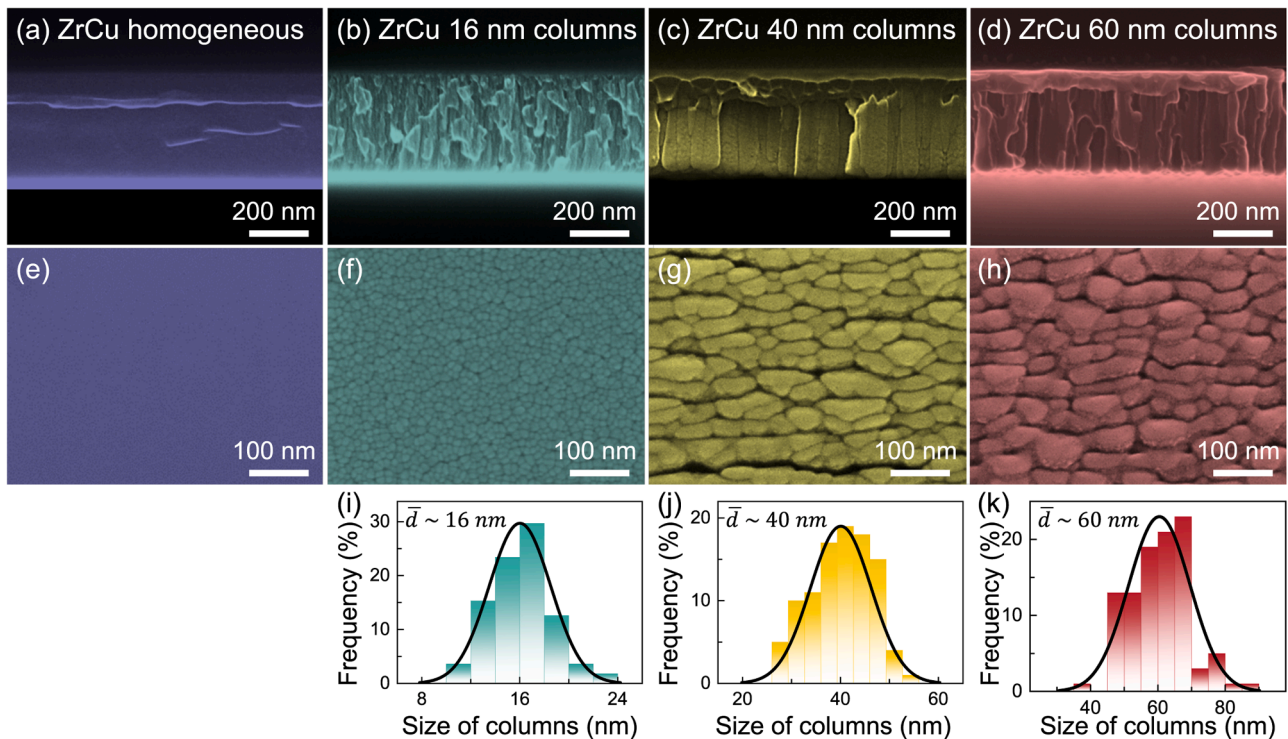

Fig. 1. Scanning electron microscopy top-view (a-d) and cross-section (e-h) micrographs displaying morphology of homogeneous (a, e), and 16 (b, f), 40 (c, g), and 60 nm (d, h) columns size ZrCu TFMGs. Size distribution of columns for 16 (i), 40 (j) and 60 nm (k) nanocolumnar ZrCu TFMGs.

to control column dimensions were achieved by employing a co-sputtering approach using pure Zr and Cu targets in the DC sputtering configuration. Under these conditions, nanocolumnar structure with an average column diameter of ~40 nm was produced (Fig. 1c, g, j, Table 1) at a working pressure of 8×10^{-1} Pa. Further optimization of the sputtering parameters, specifically increasing the power at the Cu target while maintaining the same working pressure, enabled the expansion of column diameters to ~60 nm (Fig. 1d, h, k, Table 1). This modification not only facilitated a pronounced increase in column size but also induced a change in the chemical composition of the films, with the Cu content rising to ~69 at. %.

The amorphous structure of homogeneous and nanocolumnar ZrCu TFMGs was confirmed by XRD measurements, Fig. 2 showing the presence of a broad amorphous hump which indicates the lack of long-range atomic order. The amorphous hump shifts toward higher 2θ angles increasing Cu content, as it has been already reported [16,17]. This shift reflects a reduction in average interatomic distances, attributed to compositional changes leading to the formation of shorter Cu-Cu bonds.

The presence of microscopic and macroscopic cracks which can be present in nanocolumnar films can detrimentally affect both the mechanical and electrical properties of TFMGs employed in flexible electronics. Therefore, we carried out diffusion experiments using Fe as a tracer, aiming to evaluate how structural variations influence integrity as well as atomic transport within the films. Fig. 3a shows representative concentration profiles of Fe in homogenous ZrCu TFMGs before and after annealing at 573 K. The peak position of Fe-tracer was defined as zero of depth coordinate for further analysis. Fig. 3b illustrates typical depth profiles in form of log C vs. ΔX^2 for diffusion experiments on homogeneous and 16 nm columns size TFMGs. The estimated diffusion coefficients of Fe in homogeneous and nanocolumnar TFMGs at 573 K are equal to $5.9 \times 10^{-18} \pm 0.8$ and $3.1 \times 10^{-17} \pm 1.9$ cm^2/s, respectively, indicating faster diffusion in columnar films.

3.2. Mechanical behaviour

Tensile tests of TFMG deposited on flexible substrate were performed to investigate the mechanical behavior of ZrCu homogeneous and nanocolumnar TFMGs. Fig. 4a and b depicts the evolution of crack density and COS as a function of the applied strain. Homogeneous sample is denoted by the symbol "∞" to indicate its lack of nanocolumnar structure. We show significant differences in the mechanical response between homogeneous and nanocolumnar films. Specifically,
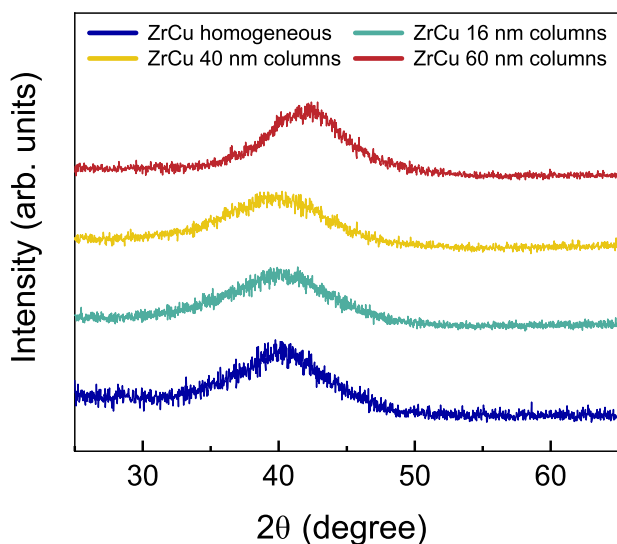

Fig. 2. XRD patterns of homogeneous and nanocolumnar ZrCu TFMGs showing a fully amorphous structure.

the COS values increase when increasing the average column diameter from 0.8 ± 0.05 % up to 1.6 ± 0.05 % for nanocolumn size of 16 and 60 nm, respectively, even exceeding those of homogeneous film (1.35 ± 0.05 %) as shown on Fig. 4b. No delamination or substrate-interface cracking was observed, indicating that cracks initiate from the free surface. This observation is consistent with the previous studies on TFMGs, which report surface-driven crack initiation under conditions of good adhesion [5,11]. Representative top-view SEM images of crack morphologies for nanocolumnar TFMGs with columns diameters of 40 and 60 nm are shown in Fig. 4c and d, respectively. For the 40 nm nanocolumnar sample (Fig. 4c), cracks predominantly follow the inter-columnar interfaces. In contrast, the nanocolumnar sample with larger column size equal to 60 nm (Fig. 4d) exhibits straighter cracks that pass through both the interfaces and the body of the columns. Further analyses of crack evolution during tensile testing, using optical microscopy, are presented in Fig. A2.

3.3. Electrical behaviour

Fig. 5a presents room-temperature electrical resistivity of ZrCu TFMGs with various size of nanocolumns, highlighting the impact of structural morphology on their electrical properties. The electrical resistivity of homogeneous ZrCu TFMG was measured to be 189.2 ± 15.3 $\mu\Omega \times$ cm, which aligns well with previously reported values in the literature [18,19].

For the nanocolumnar TFMGs, the resistivity exhibits a notable dependence on the size of the nanocolumns. Specifically, samples with the smallest nanocolumn size (16 nm) have a significantly higher resistivity of 570.0 ± 11.6 $\mu\Omega \times$ cm, compared to a homogeneous state. As the nanocolumn size increases, the resistivity gradually decreases, reaching 285.9 ± 12.6 $\mu\Omega \times$ cm for 60 nm-diameter columns (~50 % reduction compared to 16 nm columns), which is still higher than that of homogeneous TFMG.

4. Discussion

The synthesis of columnar structures has been reported for thin film metallic glasses across a range of compositions [20–23], including ZrCu-based systems [16,24,25]. However, the precise control of column size, as well as its impact on the mechanical and electrical properties of TFMGs, remains insufficiently explored.

In this work, we fabricated different nanostructured ZrCu TFMGs with tunable columns size by systematically varying the deposition parameters. Columnar growth arises from the competition between atomic-scale transport processes and geometric constraints during film growth. The two dominant mechanisms responsible for the development of columnar morphology are: (i) limited surface diffusion of adatoms or atomic clusters, and (ii) geometric shadowing induced by the directional nature of the incoming flux and the evolving surface topography [26, 27].

When surface diffusion is limited due to low substrate temperature, high working pressure, or low adatom energy, arriving adatoms or clusters cannot redistribute uniformly across the surface [23,27]. In such cases, early nucleated islands preferentially capture more material, leading to their vertical growth and promoting shadowing phenomena for adjacent lower-lying areas. As a consequence, material accumulates on the tops of growing features while shadowed regions receive significantly less flux, reinforcing the vertical separation of columns. This self-amplifying process gives rise to inclined, well-separated nanocolumns, whose tilt angle and spacing depend on the deposition geometry and flux distribution. Concurrently, competitive growth among neighboring structures further enhances this selection, as taller columns increasingly dominate the incoming flux, suppressing the growth of adjacent nuclei with lower vertical growth rates.

The characteristics of the resulting columnar structure are influenced by the combined effects of deposition parameters such as working
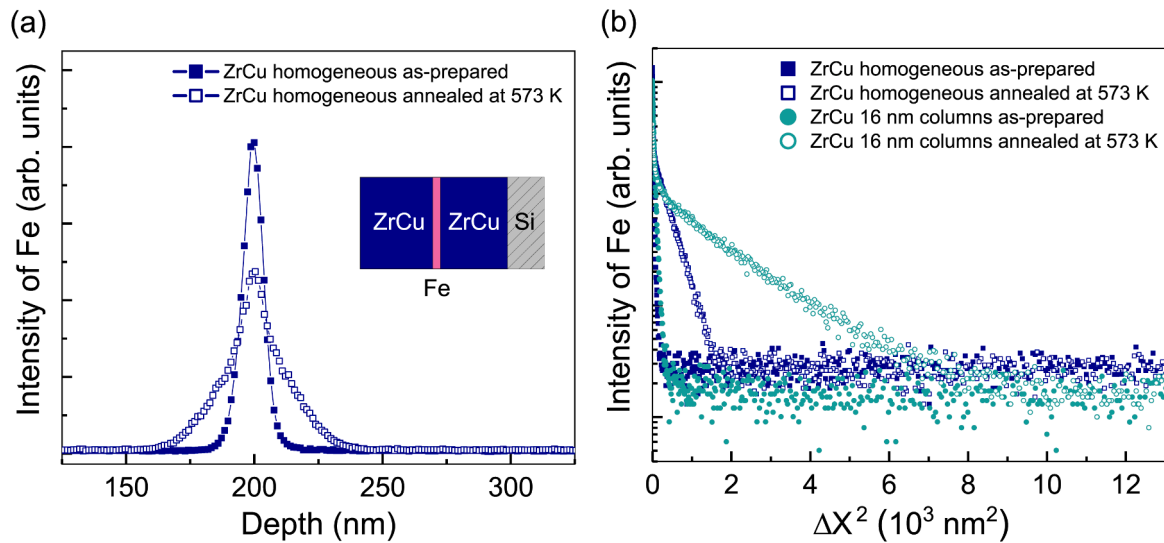
Fig. 3. (a) Scheme of the sample for diffusion measurements and concentration depth profiles in form of *C* vs. *Depth* for the diffusion of Fe in homogeneous ZrCu TFMGs in as-prepared states and after annealing at 573 K for 3.45×10^5 s. (b) Concentration depth profiles in form of log *C* vs. ΔX^2 for the diffusion of Fe in homogeneous (blue symbols) and 16 nm nanocolumnar ZrCu (teal symbols) TFMGs in as-prepared state and after diffusion annealing at 573 K for 3.45×10^5 s. Closed symbols represent the as-prepared states, while open symbols denote the annealed states.
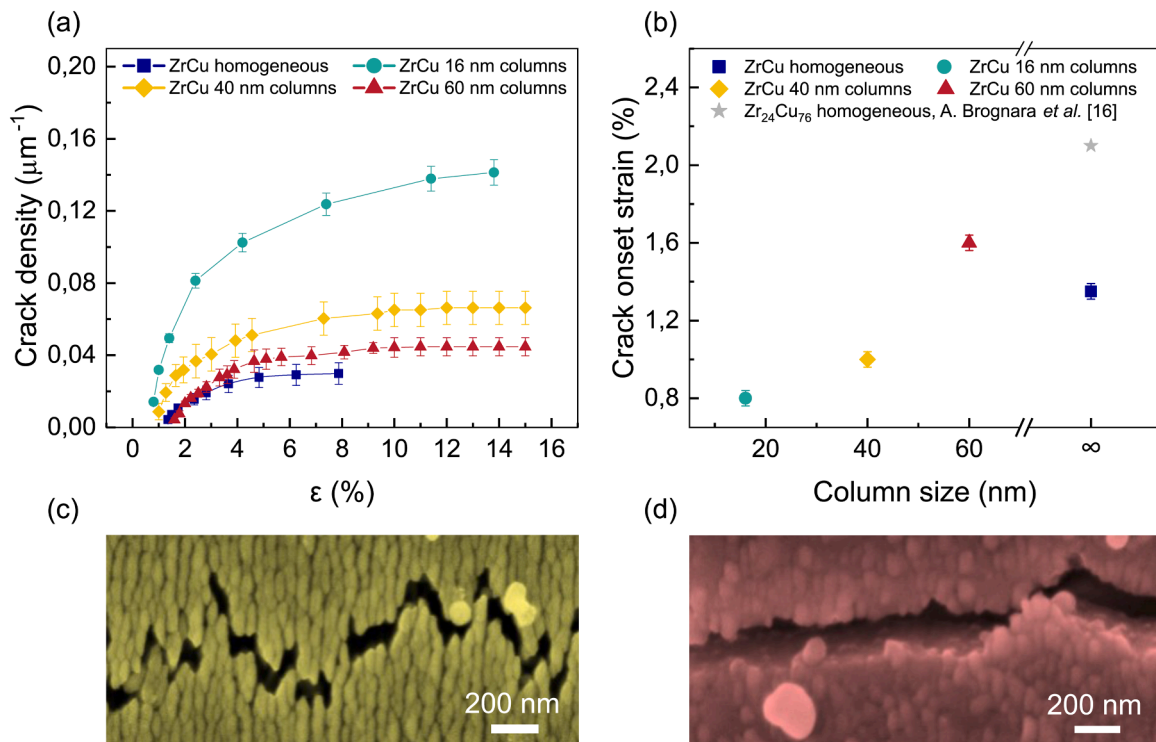

Fig. 4. Crack density vs. strain (a) and crack onset strain (b) for ZrCu homogeneous and nanocolumnar TFMGs (compared with the literature data for homogeneous $Zr_{24}Cu_{76}$ [16]). Representative top-view SEM images of crack morphologies for 40 (c) and 60 nm (d) columnar samples after the tensile tests on a flexible Kapton® substrate.

pressure, applied target power, substrate temperature, substrate tilt angle, plasma configuration (e.g., substrate biasing or HiPIMS), including magnetron field geometry. For instance, high working pressures promote the formation of atomic clusters with reduced surface mobility, which supports nucleation and shadowing-driven columnar growth [27]. Adjusting the substrate tilt angle (typically between ~15 and 40°) enhances the directionality of shadowing and allows tuning of the column inclination and separation [28]. In contrast, approaches such as substrate biasing or HiPIMS can suppress columnar growth by increasing adatom mobility through ion bombardment, leading to surface re-sputtering and densification even at oblique angles of deposition [20]. Furthermore, the use of a mirror-field magnetron configuration, where adjacent magnetrons have identical magnetic polarity may also influence the plasma density and ion-to-atom ratio near the substrate. As reported by Sproul et al. [29] mirror-field magnetron configuration tends to reduce plasma confinement and substrate ion bombardment, potentially favouring low-energy, shadowing-dominated growth regimes that contribute to the development of nanocolumnar morphology.
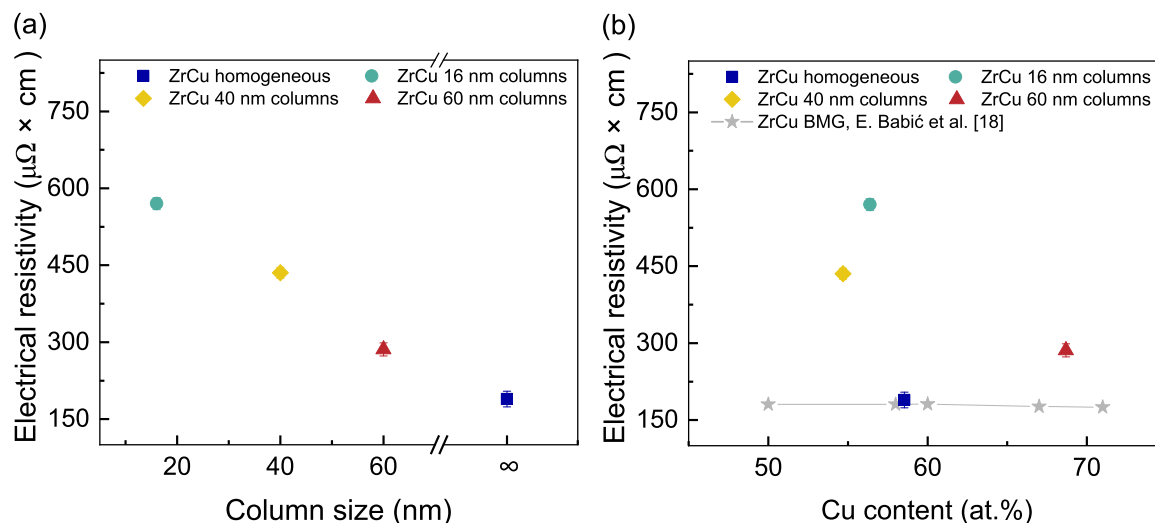
Fig. 5. Dependence of electrical resistivity of ZrCu TFMGs as a function of (a) the size of columns and (b) chemical composition (compared with literature works).

Overall, while various deposition parameters, such as substrate tilt angle, plasma configuration, and magnetron geometry, are known to affect columnar growth, this study focuses on controlling the nanocolumnar architecture of TFMGs by varying the working pressure and employing either binary or pure elemental targets. This combined strategy enables simultaneous morphological and compositional tuning, enabling the design of nanostructured film with application-specific functionalities.

In this study we show that the variation in column size of ZrCu TFMGs is attributed to the kinetic energy differences between Cu and Zr atoms or clusters during the sputtering process. These differences are primarily a result of their different atomic weights, with Cu and Zr having atomic weights of ~63.5 and 91.2 amu, respectively [30]. The higher atomic weights of Zr results in greater kinetic energy of Zr-enriched atomic clusters compared to Cu-enriched clusters, which possess lower energy and, consequently, reduced mobility on the substrate surface. This reduced mobility of Cu-rich clusters leads to the formation of larger nanocolumns with higher Cu content. A similar mechanism has been reported by Yao et al. [23], where an increase in atomic mobility, achieved by substrate heating, resulted in smaller size of nanocolumns. Our findings highlight that the reduced mobility of Cu-rich atoms or clusters contributes to the formation of larger nanocolumns, revealing a clear correlation between chemical composition and column sizes. The ability to manipulate nanocolumn dimensions by tuning deposition parameters and chemical composition offers an effective approach for fabricating nanostructured ZrCu TFMGs with tailored properties. The ability to adjust the nanocolumn size by altering the synthesis parameters as well as the chemical composition constitutes a flexible strategy for the fabrication of nanostructured ZrCu TFMGs, which has not been previously reported.

XRD measurements confirmed that the structure is amorphous and homogeneous even for nanocolumnar ZrCu TFMGs with different size of nanocolumns. This observed shift of amorphous hump toward higher *2θ* angles with increasing Cu content corresponds to a reduction in average interatomic distances, due to the formation of shorter Cu-Cu bonds. This, combined with the columnar size, plays a pivotal role in defining the structural and mechanical properties of ZrCu TFMGs.

Diffusion experiments using Fe as a tracer reveal significantly different diffusion coefficients for homogeneous and nanocolumnar films. The estimated diffusion coefficients of Fe in homogeneous and nanocolumnar TFMGs at 573 K are $5.9 \times 10^{-18} \pm 0.8$ and $3.1 \times 10^{-17} \pm 1.9$ cm²/s, respectively. These values align with the values of diffusion coefficients reported by Rigoni et al. [31] for the same alloy system, and confirm that the faster diffusion observed in columnar films is due to the presence of intercolumnar interfaces. The appearance of concentration depth profiles (intensity values saturate at some background level without reaching the substrate) indicates that the formation of cracks between the nanocolumns can be excluded [32], as their presence would lead to drastically enhanced diffusion coefficient, with the detection of the tracer through all the film thickness down to the interface with the substrate. Nevertheless, the enhanced diffusion along the interfaces can potentially be employed to decorate the interfaces with alloying elements, enabling further control over the properties of columnar TFMGs for targeted applications.

The observed variations in the mechanical and electrical properties of nanocolumnar TFMGs are attributed to the structural influence of column size and composition. As the nanocolumn size decreases, the volume fraction of intercolumnar interfaces increases, leading to a greater number of potential sites for crack initiation [33]. This explains the fact that the 16 nm nanocolumnar TFMG has the lowest value of COS (0.8 ± 0.05 %) and the highest crack density saturation. The fact that the COS is higher for 60 nm nanocolumnar films vs. homogeneous counterparts is the result of the effect of chemical composition. Higher Cu content of ~69 at. % for 60 nm nanocolumnar TFMGs leads to the formation of higher fraction of stronger Cu-Cu bonds, which affects mechanical behavior [34]. Therefore, the COS values for 60 nm nanocolumnar TFMG is greater than the corresponding one for the homogeneous counterpart with a Cu content of ~58 at. %, but lower than the COS for homogeneous ZrCu TFMGs with a Cu content of ~76 at. % and same thickness as found in the literature Ref. [16]. This highlights the complex interplay between the morphology and chemical composition of TFMGs in determining their mechanical behavior.

The electrical properties provide further insights into the effect of nanostructuring effect of ZrCu TFMGs. Fig. 5b compares the resistivity of homogeneous Zr_xCu_{100-x} TFMGs from the literature with the results obtained in this study. Homogeneous films exhibit weak dependence of electrical resistivity on the composition for the Cu concentration range from 25 to 70 at. % [18,19], suggesting that composition alone cannot account for the observed trends in nanocolumnar TFMGs. Instead, intercolumnar interfaces serve as sites for scattering of electrons, leading to an increase in electrical resistivity. The smaller column size and, consequently, a greater number of interfaces result in the highest electrical resistivity for smaller 16 nm-diameter nanocolumnar TFMGs. A similar trend is observed for crystalline materials, for which significant scattering of electrons at grain boundaries leads to increase of resistivity compared to single crystalline counterparts, and electrical resistivity increases with decreasing the grain size [35].

The dual role of intercolumnar interfaces in TFMGs is evident – they

increase electrical resistivity and reduce COS values, but they also provide opportunities for materials enhancement. For instance, the electrical resistivity of nanocolumnar TFMGs can be reduced by alloying with other elements due to enhanced atomic transport in intercolumnar interfaces or by increasing the size of columns through altering the chemical composition and/or optimizing synthesis parameters, such as working pressure, substrate temperature, subsequent heat treatment, etc. It can be assumed that for larger nanocolumns, the negative impact of the intercolumnar interfaces on the mechanical behavior can be further mitigated or even completely eliminated. This assumption is supported by results of molecular dynamic simulation of mechanical behaviour of nanoglasses with different "grain" size, showing that the presence of interfaces modifies the mechanical properties of nanoglasses only in case the average grain size does not exceed some critical size [36]. Moreover, nanocolumnar TFMGs with sufficiently large columns can potentially achieve mechanical and electrical properties comparable to those of homogeneous films, while retaining the unique advantages of their nanocolumnar architecture including the enhanced diffusion rates, which facilitate functionalization of intercolumnar interfaces with alloying elements, higher thermal stability [37], and improved biocompatibility [38]. Such features make nanocolumnar TFMGs particularly suitable for advanced applications where conventional homogeneous films might fall short.

5. Conclusions

In summary, homogenous and nanocolumnar ZrCu TFMGs with various chemical composition and nanocolumn size ranging from 16 up to 60 nm were fabricated by magnetron sputtering through a fine control of synthesis parameters (deposition pressure, applied power, use of elementary or alloyed targets). Fully amorphous nanocolumnar films are free from voids and intercolumnar cracks, as confirmed by diffusion measurements, which also report an increased diffusion coefficient. Moreover, we show that the column size, determining the volume fraction of intercolumnar interfaces, has a key influence on both mechanical and electrical properties. The ability to manipulate column size represents an effective strategy for fabricating nanostructured ZrCu TFMGs with tailored properties. Specifically, the smaller the column size, the lower crack onset strain due to the higher density of crack nucleation sites. However, nanocolumnar TFMGs with 60 nm nanocolumns demonstrate a ~20 % increase in crack onset strain compared to a homogeneous counterpart due to the reduced number of interfaces and higher fraction of stronger Cu-Cu bonds. The electrical resistivity significantly increases as the column size decreases due to the higher probability of electron scattering, with 60 nm nanocolumnar TFMGs reporting the smallest increase of electrical resistivity (~50 %) compared to the homogeneous counterpart. The present study can open the way for future research on nanoengineering TFMGs with nanocolumnar structure and decorated interfaces to achieve improved combination of mechanical and electrical performance with practical implications for different research domains especially for flexible electronics.

CRediT authorship contribution statement

Evgeniy Boltynjuk: Writing – review & editing, Visualization, Validation, Methodology, Investigation, Formal analysis, Data curation, Conceptualization. **Francesco Bignoli:** Writing – review & editing, Validation, Methodology, Investigation, Formal analysis. **Sree Harsha Nandam:** Writing – review & editing, Investigation. **Damien Faurie:** Writing – review & editing, Resources, Formal analysis. **Alexander Welle:** Writing – review & editing, Resources, Methodology, Formal analysis. **Robert Kruk:** Writing – review & editing. **Philippe Djemia:** Writing – review & editing, Project administration, Funding acquisition. **Horst Hahn:** Writing – review & editing, Supervision, Resources, Project administration, Methodology, Funding acquisition, Conceptualization. **Yulia Ivanisenko:** Writing – review & editing, Supervision, Project administration, Methodology, Funding acquisition, Conceptualization. **Matteo Ghidelli:** Writing – review & editing, Writing – original draft, Supervision, Resources, Project administration, Methodology, Funding acquisition, Conceptualization.

Declaration of competing interest

The authors declare that they have no known competing financial interests or personal relationships that could have appeared to influence the work reported in this paper.

Acknowledgements

Appendices

A1. The influence of varying synthesis parameters using RF sputtering on the column size of ZrCu TFMGs

Synthesis parameters (working pressure, sputtering power, substrate temperature) of RF sputtering were varied to obtain columnar ZrCu TFMGs with various size of columns. All the synthesis parameters and resulting size of columns are listed in Table A1.

Table A1
Synthesis details of columnar CuZr TFMGs deposited by RF magnetron sputtering.

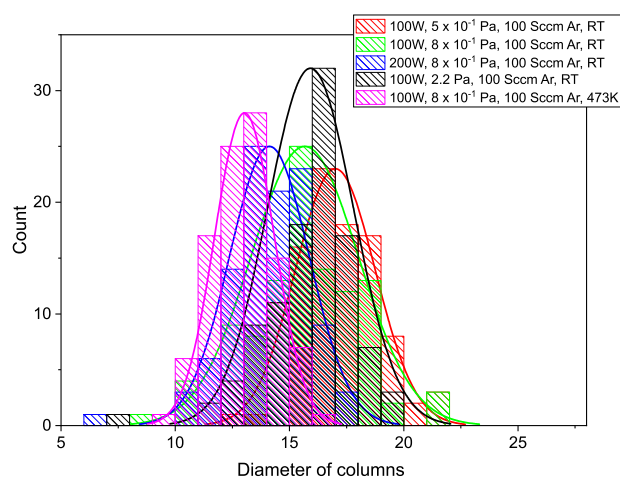| Size of columns, nm	Working pressure, Pa	Sputtering power, W	Substrate temperature, K
17 ± 1.7	5×10^{-1}	100	298
15.7 ± 2.1	8×10^{-1}	100	298
14.2 ± 1.5	8×10^{-1}	200	298
16 ± 1.6	2.2×10^{0}	100	298
13 ± 1.3	8×10^{-1}	100	473

Fig. A1. Column size distribution of ZrCu TFMGs deposited by RF magnetron sputtering (under the conditions mentioned in Table A1).

A2. Images of crack evolution during tensile testing of ZrCu TFGMs deposited on a flexible Kapton® substrate
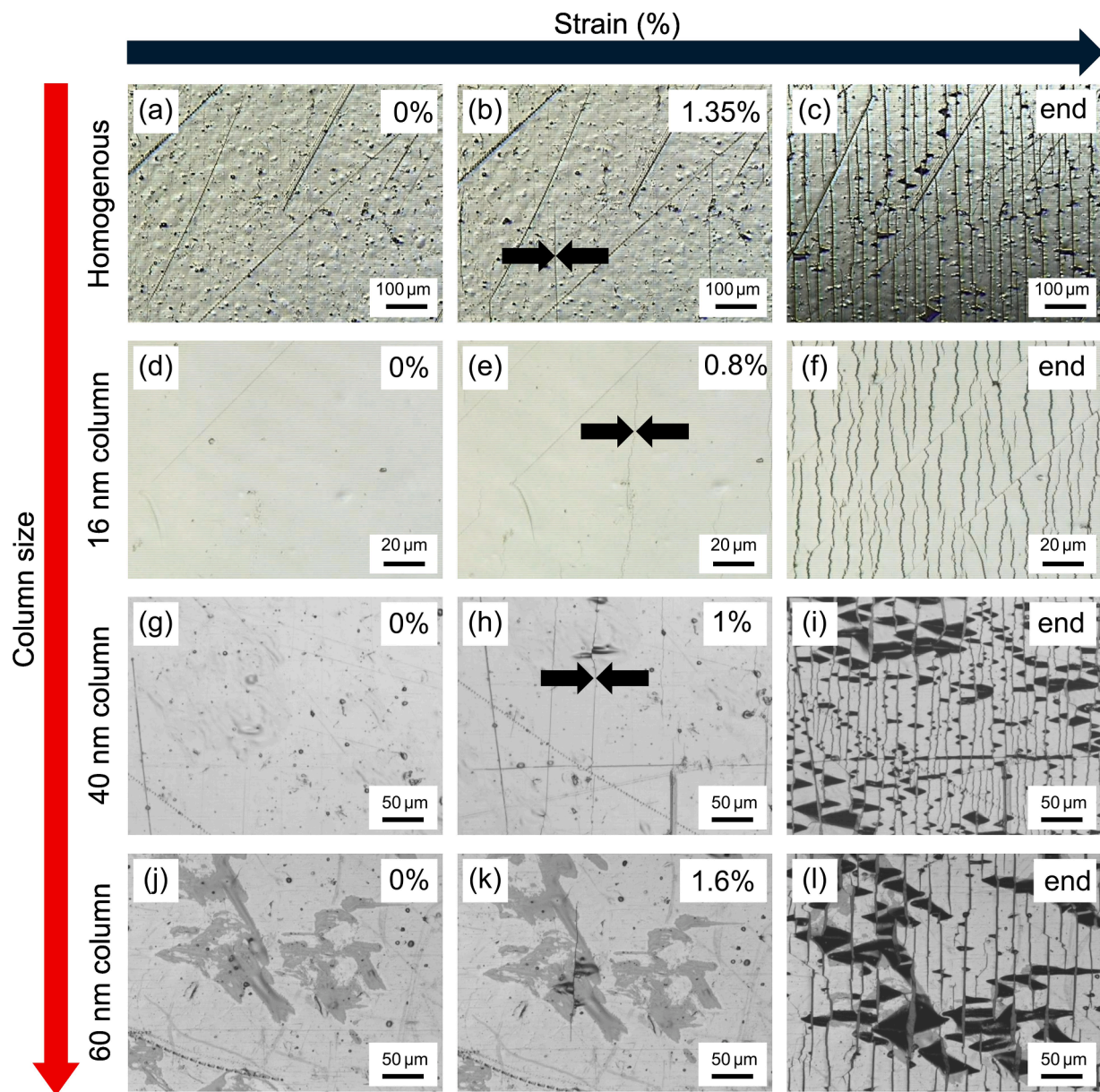

Fig. A2. Top-view optical microscopy images of crack evolution during tensile testing of ZrCu TFGMs deposited on a flexible Kapton® substrate: (a, b, c) homogeneous film; (d, e, f) columnar film with columns of 16 nm; (g, h, i) columnar film with columns of 40 nm and (j, k, l) columnar film with columns of 60 nm. The vertical left side of the panel shows images of films before the deformation. Images in the central part show images of films reaching crack onset strain. The vertical right side of the panel shows images of films when film buckling appeared.

Data availability

Data will be made available on request.

References

[1] D. Corzo, G. Tostado-Blázquez, D. Baran, Flexible Electronics: status, challenges and opportunities, Front. Electron. 1 (2020) 594003, https://doi.org/10.3389/felec.2020.594003.

[2] W. Wu, Stretchable electronics: functional materials, fabrication strategies and applications, Sci. Technol. Adv. Mater. 20 (2019) 187–224, https://doi.org/10.1080/14686996.2018.1549460.

[3] M.J. Cordill, P. Kreiml, C. Mitterer, Materials engineering for flexible metallic thin film applications, Materials 15 (2022) 926, https://doi.org/10.3390/ma15030926.

[4] J.P. Chu, J.S.C. Jang, J.C. Huang, H.S. Chou, Y. Yang, J.C. Ye, Y.C. Wang, J.W. Lee, F.X. Liu, P.K. Liaw, Y.C. Chen, C.M. Lee, C.L. Li, C. Rullyani, Thin film metallic glasses: unique properties and potential applications, Thin Solid Films 520 (2012) 5097–5122, https://doi.org/10.1016/j.tsf.2012.03.092.

[5] P. Yiu, W. Diyatmika, N. Bönninghoff, Y.-C. Lu, B.-Z. Lai, J.P. Chu, Thin film metallic glasses: properties, applications and future, J. Appl. Phys. 127 (2020) 030901, https://doi.org/10.1063/1.5122884.

[6] M. Ghidelli, H. Idrissi, S. Gravier, J.-J. Blandin, J.-P. Raskin, D. Schryvers, T. Pardoen, Homogeneous flow and size dependent mechanical behavior in highly ductile Zr65Ni35 metallic glass films, Acta Mater. 131 (2017) 246–259, https://doi.org/10.1016/j.actamat.2017.03.072.

[7] K.H.J. Buschow, N.M. Beekmans, Thermal stability and electronic properties of amorphous Zr-Co and Zr-Ni alloys, Phys. Rev. B 19 (1979) 3843–3849, https://doi.org/10.1103/PhysRevB.19.3843.

[8] Bulk Metallic Glasses, 2nd Edition, CRC Press, 2017, https://doi.org/10.1201/9781315153483.

[9] J. Antonowicz, A. Pietnoczka, K. Pękała, J. Latuch, G.A. Evangelakis, Local atomic order, electronic structure and electron transport properties of Cu-Zr metallic glasses, J. Appl. Phys. 115 (2014) 203714, https://doi.org/10.1063/1.4879903.

[10] H.J. Xian, C.R. Cao, J.A. Shi, X.S. Zhu, Y.C. Hu, Y.F. Huang, S. Meng, L. Gu, Y. H. Liu, H.Y. Bai, W.H. Wang, Flexible strain sensors with high performance based on metallic glass thin film, Appl. Phys. Lett. 111 (2017) 121906, https://doi.org/10.1063/1.4993560.

[11] O. Glushko, M. Mühlbacher, C. Gammer, M.J. Cordill, C. Mitterer, J. Eckert, Exceptional fracture resistance of ultrathin metallic glass films due to an intrinsic size effect, Sci. Rep. 9 (2019) 8281, https://doi.org/10.1038/s41598-019-44384-z.

[12] M. Jung, E. Lee, D. Kim, K. Kim, C. Yun, H. Lee, H. Kim, K. Rhie, S. Jeon, Amorphous FeZr metal for multi-functional sensor in electronic skin, Npj Flex. Electron. 3 (2019) 8, https://doi.org/10.1038/s41528-019-0051-7.

[13] M. Ghidelli, A. Orekhov, A.L. Bassi, G. Terraneo, P. Djemia, G. Abadias, M. Nord, A. Béché, N. Gauquelin, J. Verbeeck, J.-P. Raskin, D. Schryvers, T. Pardoen, H. Idrissi, Novel class of nanostructured metallic glass films with superior and tunable mechanical properties, Acta Mater 213 (2021) 116955, https://doi.org/10.1016/j.actamat.2021.116955.

[14] S. Lee, S.-W. Kim, M. Ghidelli, H.S. An, J. Jang, A.L. Bassi, S.-Y. Lee, J.-U. Park, Integration of transparent supercapacitors and electrodes using nanostructured metallic glass films for wirelessly rechargeable, skin heat patches, Nano Lett. 20 (2020) 4872–4881, https://doi.org/10.1021/acs.nanolett.0c00869.

[15] H. Hahn, R.S. Averback, Dependence of tracer diffusion on atomic size in amorphous Ni-Zr, Phys. Rev. B 37 (1988) 6533–6535, https://doi.org/10.1103/PhysRevB.37.6533.

[16] A. Brognara, J.P. Best, P. Djemia, D. Faurie, G. Dehm, M. Ghidelli, Effect of composition and nanostructure on the mechanical properties and thermal stability of Zr100-xCux thin film metallic glasses, Mater. Des. 219 (2022) 110752, https://doi.org/10.1016/j.matdes.2022.110752.

[17] M. Apreutesei, P. Steyer, L. Joly-Pottuz, A. Billard, J. Qiao, S. Cardinal, F. Sanchette, J.M. Pelletier, C. Esnouf, Microstructural, thermal and mechanical behavior of co-sputtered binary Zr–Cu thin film metallic glasses, Thin Solid Films 561 (2014) 53–59, https://doi.org/10.1016/j.tsf.2013.05.177.

[18] E. Babić, K. Šaub, Coherent effects in conductivity of glassy ZrCu alloys, in: P. Grosse (Ed.), Festkörperprobleme 25, Springer Berlin Heidelberg, Berlin, Heidelberg, 1985, pp. 485–492, https://doi.org/10.1007/BFb0108183.

[19] P. Zeman, M. Zítek, Š. Zuzjaková, R. Čerstvý, Amorphous Zr-Cu thin-film alloys with metallic glass behavior, J. Alloys Compd. 696 (2017) 1298–1306, https://doi.org/10.1016/j.jallcom.2016.12.098.

[20] N. Bönninghoff, W. Diyatmika, J.P. Chu, S. Mráz, J.M. Schneider, C.-L. Lin, F. Eriksson, G. Greczynski, ZrCuAlNi thin film metallic glass grown by high power impulse and direct current magnetron sputtering, Surf. Coat. Technol. 412 (2021) 127029, https://doi.org/10.1016/j.surfcoat.2021.127029.

[21] Y.H. Liu, T. Fujita, A. Hirata, S. Li, H.W. Liu, W. Zhang, A. Inoue, M.W. Chen, Deposition of multicomponent metallic glass films by single-target magnetron sputtering, Intermetallics 21 (2012) 105–114, https://doi.org/10.1016/j.intermet.2011.10.007.

[22] S.V. Ketov, R. Joksimovic, G. Xie, A. Trifonov, K. Kurihara, D.V. Louzguine-Luzgin, Formation of nanostructured metallic glass thin films upon sputtering, Heliyon 3 (2017) e00228, https://doi.org/10.1016/j.heliyon.2016.e00228.

[23] W. Yao, Q.P. Cao, S.Y. Liu, X.D. Wang, H.J. Fecht, A. Caron, D.X. Zhang, J.Z. Jiang, Tailoring nanostructured Ni-Nb metallic glassy thin films by substrate temperature, Acta Mater 194 (2020) 13–26, https://doi.org/10.1016/j.actamat.2020.04.046.

[24] H. Voigt, A. Rigoni, E. Boltynjuk, M.R. Chellali, B. Tyler, H. Rösner, S. Divinski, H. Hahn, G. Wilde, Evidence for glass–glass interfaces in a columnar Cu–Zr nanoglass, Adv. Funct. Mater. 33 (2023) 2302386, https://doi.org/10.1002/adfm.202302386.

[25] A. Borroto, S. Bruyère, S. Migot, C. De Melo, D. Horwat, J.F. Pierson, Nanostructured Zr-Cu metallic glass thin films with tailored electrical and optical properties, J. Alloys Compd. 967 (2023) 171681, https://doi.org/10.1016/j.jallcom.2023.171681.

[26] J.A. Thornton, Influence of apparatus geometry and deposition conditions on the structure and topography of thick sputtered coatings, J. Vac. Sci. Technol. 11 (1974) 666–670, https://doi.org/10.1116/1.1312732.

[27] G.S. Bales, A. Zangwill, Macroscopic model for columnar growth of amorphous films by sputter deposition, J. Vac. Sci. Technol. Vac. Surf. Films 9 (1991) 145–149, https://doi.org/10.1116/1.577116.

[28] R. Kowong, S. Denchitcharoen, T. Lertvanithphol, N. Triamnak, C. Chananonnawathorn, K. Jaruwongrungsee, A. Klamchuen, P. Muthitamongkol, W. Phae-ngam, H. Nakajima, P. Songsiririththigul, M. Horprathum, Nanostructure optimization of Zr-W-Ti metallic glass thin films via multitarget co-sputtering with oblique angle deposition approach, J. Alloys Compd. 886 (2021) 161265, https://doi.org/10.1016/j.jallcom.2021.161265.

[29] W.D. Sproul, P.J. Rudnik, M.E. Graham, S.L. Rohde, High rate reactive sputtering in an opposed cathode closed-field unbalanced magnetron sputtering system, Surf. Coat. Technol. 43–44 (1990) 270–278, https://doi.org/10.1016/0257-8972(90)90080-V.

[30] S.S. Sakhonenkov, E.O. Filatova, Nanoscale W/Be multilayers: intermixing during magnetron sputtering deposition and effect of heat treatment, Appl. Surf. Sci. 571 (2022) 151265, https://doi.org/10.1016/j.apsusc.2021.151265.

[31] C. Aaron Rigoni, E. Boltynjuk, H. Voigt, H. Rösner, B. Tyler, H. Hahn, S.V. Divinski, G. Wilde, Enhanced diffusion in thin-film Cu-Zr nanoglasses, Acta Mater. 265 (2024) 119634, https://doi.org/10.1016/j.actamat.2023.119634.

[32] J. Ribbe, D. Baither, G. Schmitz, S.V. Divinski, Network of porosity formed in ultrafine-grained copper produced by equal channel angular pressing, Phys. Rev. Lett. 102 (2009) 165501, https://doi.org/10.1103/PhysRevLett.102.165501.

[33] K. Wu, Y.Q. Wang, H.Z. Yuan, J.Y. Zhang, G. Liu, J. Sun, Fragmentation and adhesion properties of Cu-Zr amorphous thin films on polyimide substrates, Philos. Mag. Lett. 98 (2018) 464–472, https://doi.org/10.1080/09500839.2019.1575529.

[34] Y.Q. Cheng, A.J. Cao, H.W. Sheng, E. Ma, Local order influences initiation of plastic flow in metallic glass: effects of alloy composition and sample cooling history, Acta Mater 56 (2008) 5263–5275, https://doi.org/10.1016/j.actamat.2008.07.011.

[35] I. Bakonyi, Accounting for the resistivity contribution of grain boundaries in metals: critical analysis of reported experimental and theoretical data for Ni and Cu, Eur. Phys. J. Plus 136 (2021) 410, https://doi.org/10.1140/epjp/s13360-021-01303-4.

[36] K. Albe, Y. Ritter, D. Şopu, Enhancing the plasticity of metallic glasses: shear band formation, nanocomposites and nanoglasses investigated by molecular dynamics simulations, Mech. Mater. 67 (2013) 94–103, https://doi.org/10.1016/j.mechmat.2013.06.004.

[37] N. Chen, D.V. Louzguine-Luzgin, G.Q. Xie, P. Sharma, J.H. Perepezko, M. Esashi, A. R. Yavari, A. Inoue, Structural investigation and mechanical properties of a representative of a new class of materials: nanograined metallic glasses, Nanotechnology 24 (2013) 045610, https://doi.org/10.1088/0957-4484/24/4/045610.

[38] N. Chen, X. Shi, R. Witte, K.S. Nakayama, K. Ohmura, H. Wu, A. Takeuchi, H. Hahn, M. Esashi, H. Gleiter, A. Inoue, D.V. Louzguine, A novel Ti-based nanoglass composite with submicron–nanometer-sized hierarchical structures to modulate osteoblast behaviors, J. Mater. Chem. B 1 (2013) 2568, https://doi.org/10.1039/c3tb20153h.